1 Supporting information

Correlation of MOF-808 parameters to mixed-matrix membrane CO_2 permeation behavior

Raymond Thür[a], Daan Van Havere[a], Niels Van Velthoven[a], Simon Smolders[a], Aran Lamaire[b], Jelle Wieme[b], Veronique Van Speybroeck[b], Dirk De Vos[a], Ivo F.J. Vankelecom[a]

[a]Centre for Membrane Separations, Adsorption, Catalysis and Spectroscopy for Sustainable Solutions (cMACS), KU Leuven, Celestijnenlaan 200F, Box 2454, 3001 Heverlee, Belgium
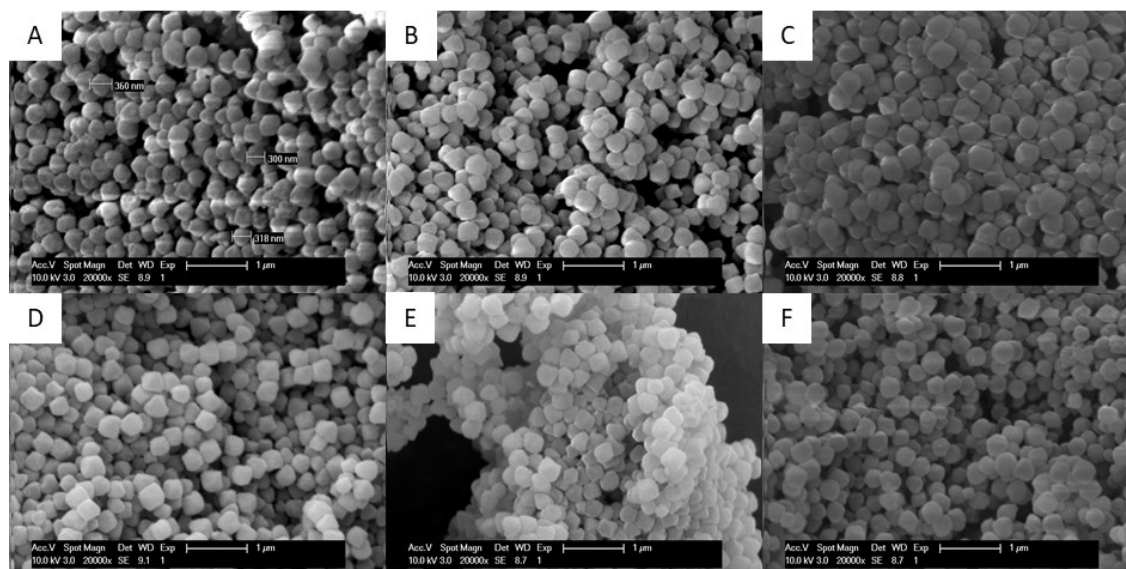
[b]Center for Molecular Modeling, Ghent University, Tech Lane Ghent Science Park, Campus A, Technologiepark 46, 9052 Zwijnaarde, Belgium

E-mail: ivo.vankelecom@kuleuven.be
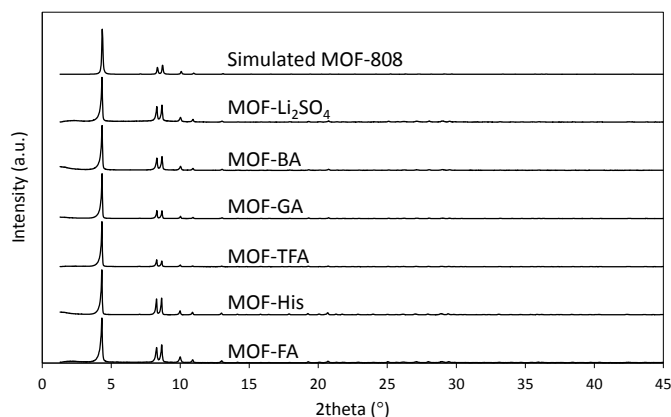
Figure S1: XRD patterns of all MOF samples.

Figure S2: SEM images of all MOF particles: (A) MOF-FA, (B) MOF-GA, (C) MOF-His, (D) MOF-BA, (E) MOF-TFA and (F) MOF-Li$_2$SO$_4$.

Table S1: Average size of all MOFs calculated after ImageJ analysis. 30 samples were measured per MOF.

	Number	Average size (nm)	Variance
MOF-BA	30	362.7	2132.1
MOF-FA	30	346.6	1080.2
MOF-GA	30	352.1	813.32
MOF-His	30	355.5	1786.3
MOF-Li$_2$SO$_4$	30	336.7	1131.8
MOF-TFA	30	347.8	914.24

Table S2: ANOVA analysis of the MOF particle sizes. As the p-value is larger than the significance level (0.05), no statistically significant difference in size exists between the samples.
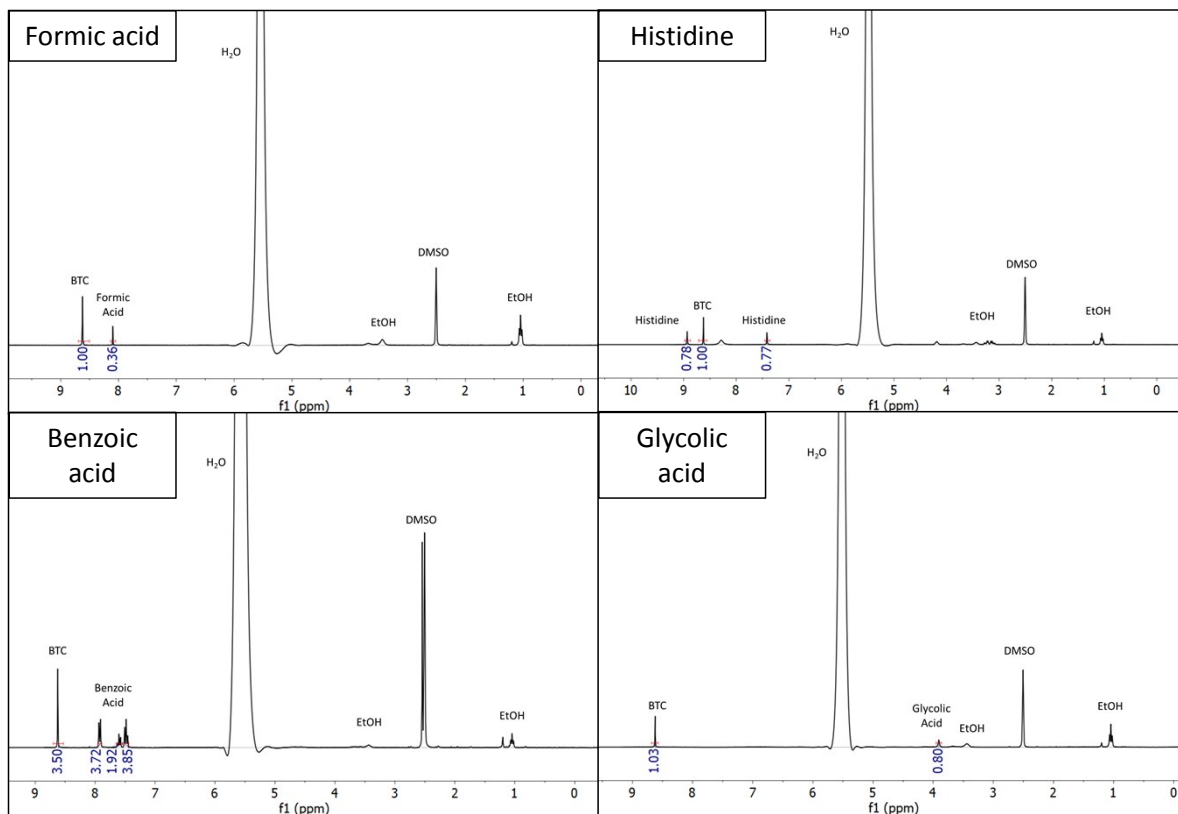
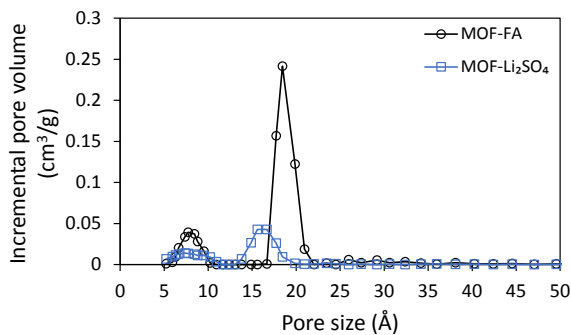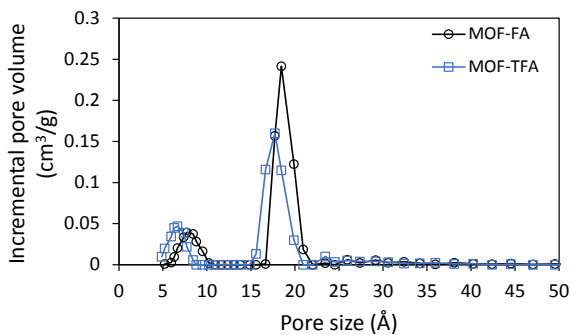| ANOVA						
Source of Variation	SS	df	MS	F	p-value	F crit
Between Groups	11680.1	5	2336	1.7837	0.1185	2.2661
Within Groups	227882	174	1310			
Total	239562	179				

21
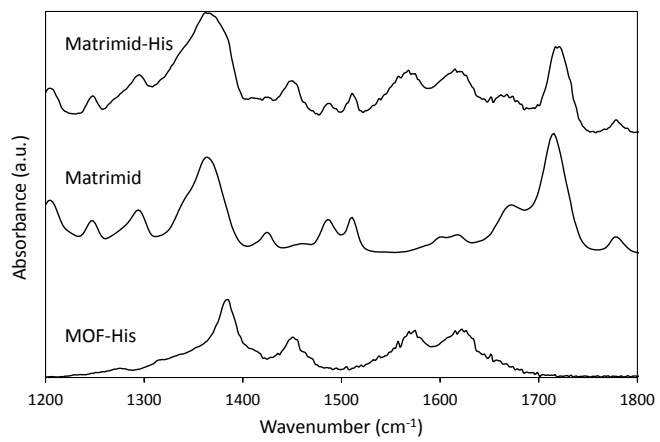
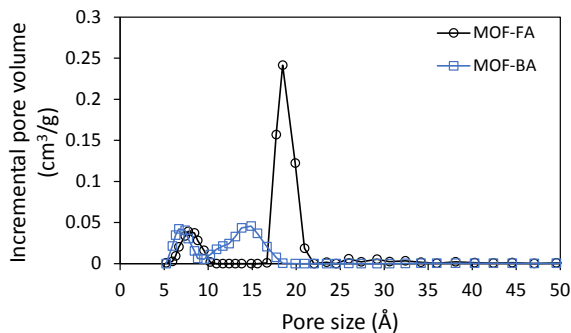Figure S3: ATR-FTIR spectrum of MMM-His, Matrimid and MOF-His.

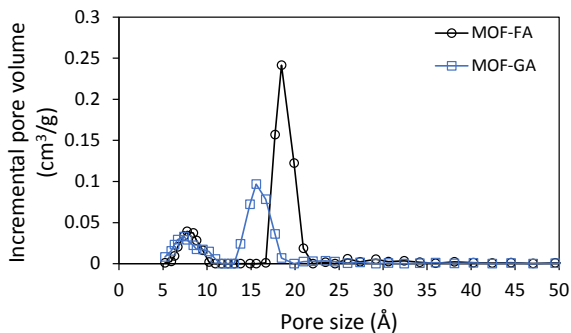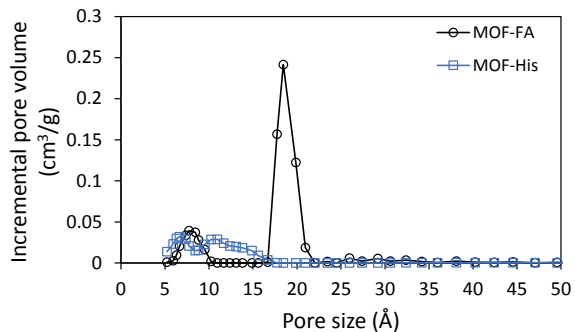22

23

Figure S4: ^{1}H-NMR spectra for MOF-FA, MOF-BA, MOF-His and MOF-GA.

25

26

27

Figure S5: Incremental pore volume as a function of pore size for all MOFs.

29
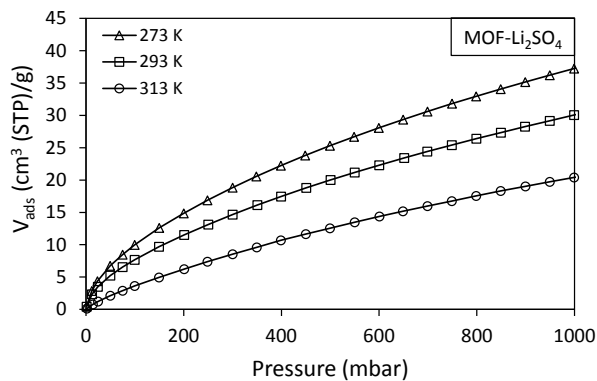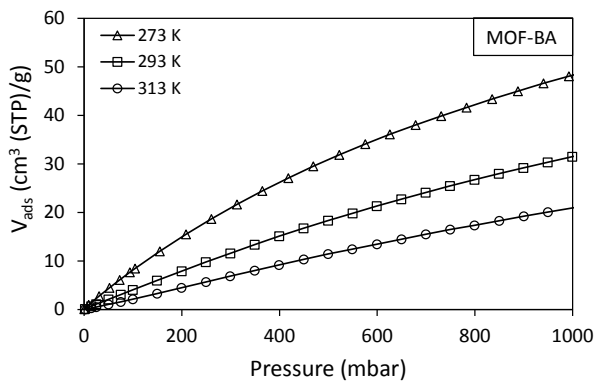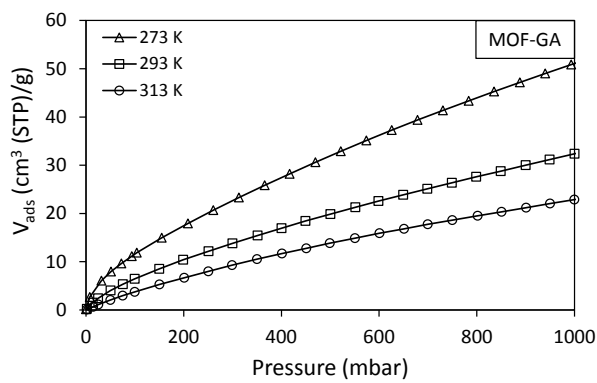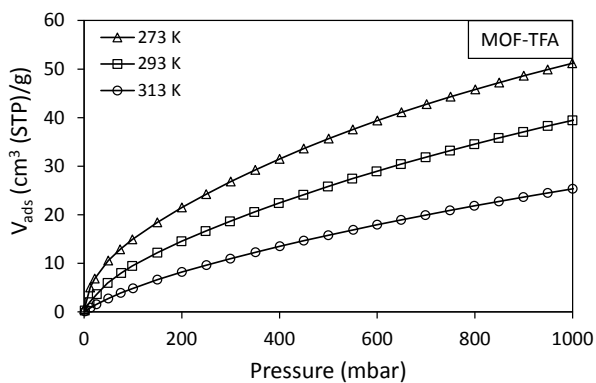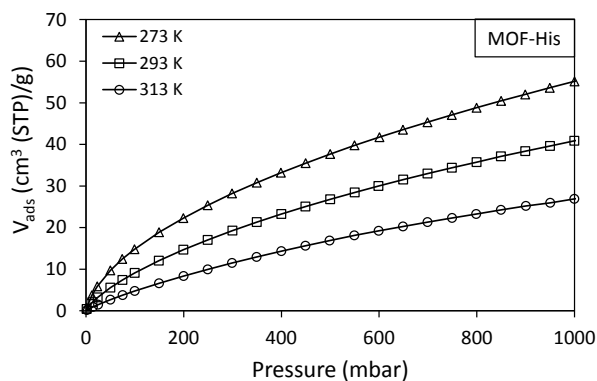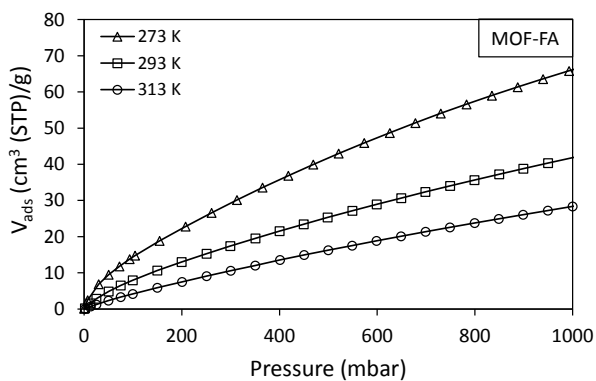
Figure S6: CO_2 uptake of all MOFs at 273 K, 293 K and 313 K.
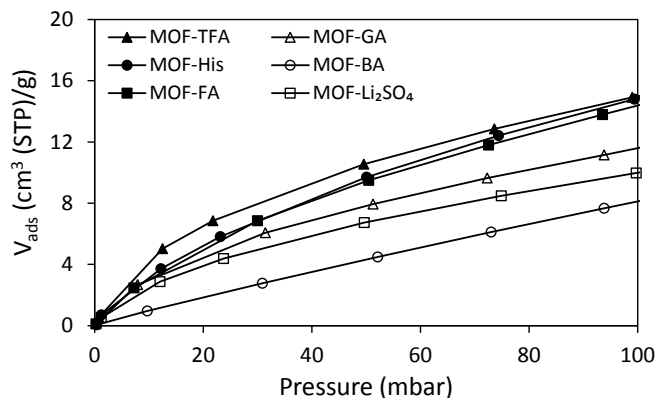
31

32 Figure S7: CO_2 adsorption isotherms of all MOFs in the low-pressure region (0-100 mbar) at 273 K.

33 Table S3: Model parameters for the dual-site Langmuir fit on the CO_2 adsorption isotherm at 273 K. N is the amount of adsorbed
34 gas (cm³ (STP)/g), $N_{m,A}$ and $N_{m,B}$ the amount of adsorbed gas at saturation for sorption site A and B, respectively (cm³ (STP)/g) and
35 b_A and b_B the adsorption equilibrium constants for, respectively, sorption site A and B. R^2 is the correlation coefficient.

	$N_{m,A}$	$N_{m,B}$	b_A	b_B	R^2
MOF-FA	0.34	8.74	0.046	0.00042	1.0000
MOF-GA	0.32	8.14	0.048	0.00031	1.0000
MOF-BA	0.04	4.95	0.014	0.00073	1.0000
MOF-TFA	0.43	4.44	0.056	0.00070	1.0000
MOF-His	0.59	5.59	0.020	0.00050	0.9999
MOF-Li$_2$SO$_4$	0.35	3.87	0.028	0.00051	0.9999

36

37 Table S4: CO_2 Q_{st} (kJ/mol) of all MOFs for different CO_2 loadings (0, 5, 15, 30 cm³ (STP)/g).

	CO_2 adsorbed (cm³ (STP)/g)			
	0	**5**	**15**	**30**
MOF-FA	30.9	34.1	25.6	22.1
MOF-His	31.8	30.1	25.6	22.4
MOF-TFA	39.2	37.2	27.7	22.5
MOF-GA	37.6	32.9	22.6	21.4
MOF-BA	23.9	22.8	21.8	20.7
MOF-Li$_2$SO$_4$	28.2	28.0	20.3	18.3

38 Table S5: Solubility (S) of CO_2 and N_2 in the Matrimid reference membrane and the MMMs. S_{CO2}/S_{N2} constitutes the CO_2/N_2
39 solubility selectivity. Measurements were conducted at 30 °C and varying pressures (see table).

40

41

42

43

44

45

Pressure (bar)	**Membrane**	S_{N2}	S_{CO2}	S_{CO2}/S_{N2}

|				
	Matrimid	0.00703	0.08125	11.6
	MMM-GA	0.00788	0.09487	12.0
	MMM-His	0.00809	0.10152	12.5
5	MMM-FA	0.00694	0.10454	15.1
	MMM-BA	0.00578	0.10036	17.4
	MMM-TFA	0.00609	0.10828	17.8
	MMM-Li$_2$SO$_4$	0.00592	0.10901	18.4
	Matrimid	0.00594	0.05615	9.45
	MMM-GA	0.00675	0.06699	9.92
	MMM-His	0.00692	0.06833	9.87
10	MMM-FA	0.00586	0.07399	12.6
	MMM-BA	0.00571	0.06989	12.2
	MMM-TFA	0.00524	0.07603	14.5
	MMM-Li$_2$SO$_4$	0.00536	0.07594	14.2
	Matrimid	0.00537	0.04539	8.46
	MMM-GA	0.00637	0.05398	8.46
	MMM-His	0.00611	0.05410	8.85
15	MMM-FA	0.00515	0.06053	11.8
	MMM-BA	0.00529	0.05572	10.5
	MMM-TFA	0.00454	0.06277	13.8
	MMM-Li$_2$SO$_4$	0.00472	0.06062	12.9

46

47 **Force fields**

48 To perform static GCMC (Grand Canonical Monte Carlo) simulations for the differently functionalized

49 MOF-808 structures, each structure was parametrized by a non-covalent force field that contains both

50 electrostatic and van der Waals interactions:

51 $V = V_{ei} + V_{vdW}$ (Equation 8)

52 The electrostatic interactions are modelled by a Coulomb interaction between Gaussian charge

53 distributions, which are derived from cluster models of the MOF-808 Zr$_6$O$_8$H$_x$ brick, using phenyl

54 terminations at the positions of the six BTC^{3-} linkers (Figure S8). After a geometry optimization with

55 Gaussian 16[82], using the B3LYP functional[83] and 6-311g(d,p) basis sets[84] for all atoms but zirconium, for

56 which the LanL2DZ basis set and pseudopotential are used[85], the electron density of the cluster is

57 determined with gpaw[86] using the PBE functional[33]. Finally, the atomic charges q$_i$ are derived with the

58 Minimal Basis Iterative Stockholder (MBIS) partitioning scheme[87], so that the electrostatic interaction is

59 given by

60 $$V_{ei} = \frac{1}{2} \sum_{\substack{i,j = 1 \\ (i \neq j)}} \frac{q_i q_j}{4\pi\epsilon_0 r_{ij}} erf\left(\frac{r_{ij}}{d_{ij}}\right)$$ (Equation 9)

61 with r_{ij} the distance between atoms i and j, and q_i and d_i respectively the total charge and the radius of

62 the Gaussian charge distribution[88] centered on atom i. The mixed radius d_{ij} of the Gaussian charges is

63 given by $\sqrt{d_i^2 + d_j^2}$.

(a)   **(b)**
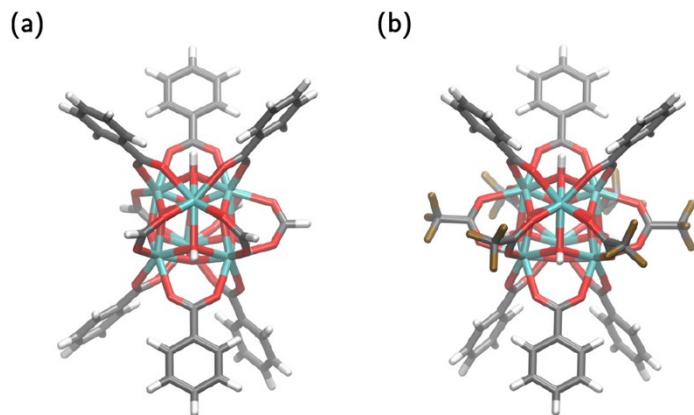
64

65 Figure S8: Cluster models used in the derivation of the atomic charges of (a) MOF-FA-def1 and (b) MOF-TFA.

66 The van der Waals interactions are modelled by a Lennard-Jones potential:

67
$$V_{vdW} = \sum_{i<j} 4\epsilon_{ij}\left[\left(\frac{\sigma_{ij}}{r_{ij}}\right)^{12} - \left(\frac{\sigma_{ij}}{r_{ij}}\right)^6\right]$$
(Equation 10)

68 for which the parameters σ_{ij} and ϵ_{ij} between atom i and j are derived from the atomic DREIDING

69 parameters[41] (and UFF parameters[43] for zirconium), using the Lorentz-Berthelot mixing rules:

70
$$\sigma_{ij} = \frac{\sigma_i + \sigma_j}{2} \text{ and } \epsilon_{ij} = \sqrt{\epsilon_i \epsilon_j}$$
(Equation 11)

71 In the GCMC simulations, the Lennard-Jones interactions are truncated at 10.1 Å and complemented by
72 the appropriate tail corrections.

73 **Modelled CO_2 isotherms**

74 The CO_2 adsorption isotherms obtained from GCMC simulations at different pressures for MOF-FA and

75 MOF-TFA are given in Figure S9. The isotherms for both MOF-FA and MOF-TFA are similar to the

76 experimental ones, although small differences can be observed. These can be attributed to the different

77 number of modulator molecules on the zirconium cluster and the slightly higher temperature at which

78 CO_2 adsorption was simulated. For MOF-FA, two defect structures with, respectively, one and three

79 missing formate groups per zirconium cluster are modelled next to the pristine MOF-FA (containing six

80 formate groups per cluster). The absolute differences (i.e. the number of adsorbed CO_2 molecules per unit

81 cell) between the pristine and defects structures are small and only significant at higher pressures.

82 However, per unit of mass, this results in a slightly larger uptake for MOF-FA with three defects in

83 comparison to pristine MOF-FA.
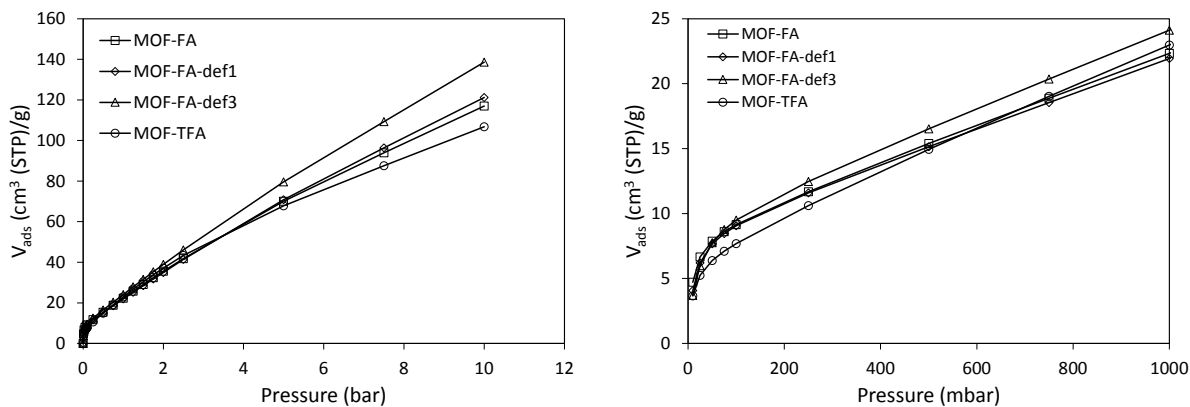
84

85 Figure S9: Modelled CO_2 adsorption isotherms for MOF-FA and MOF-TFA. For MOF-FA, the number of defects (i.e. absence of
86 formate molecule) on the zirconium clusters has been varied from one (MOF-FA-def1) to three (MOF-FA-def3).
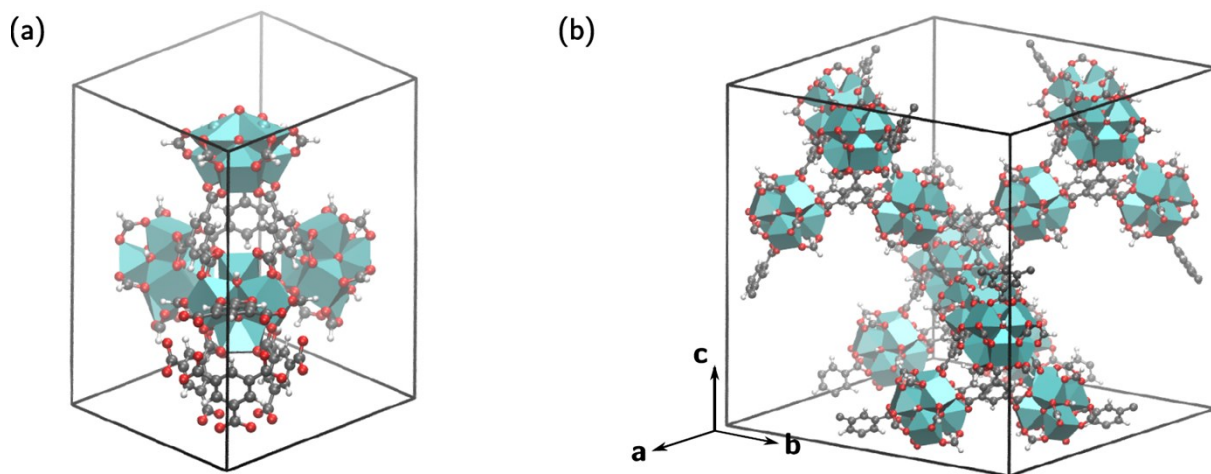

87

88 Figure S10: (a) Primitive unit cell of MOF-FA. (b) Conventional cubic unit cell of MOF-FA.

89 The CO_2 density in MOF-FA-def1 exhibits only small differences in comparison with the pristine MOF-FA.

90 MOF-FA-def3, on the other hand, does show some interesting differences (Figure S10). Similar to MOF-

91 FA, the CO_2 molecules are first adsorbed in the cages of the linkers, yielding a square grid of adsorption

92 sites when viewing MOF-808 along the c-axis. The second type of adsorption sites, covering the open sides

93 of the linkers, become more prominently occupied with increasing pressure, but do not longer give rise

94 to a square grid of adsorption sites. This is due to the fact that an additional type of adsorption sites is

95 present in MOF-FA-def3, located on the open metal sites of the zirconium clusters (marked as site 3 in

96 Figure S10). These adsorption sites are observed to be more favorable than the adsorption sites located

97 at the linkers. With increasing pressure the MOF-808 structure exhibits a different encapsulation, which

98 is primarily formed by the adsorption sites at the open metal sites and the adsorption sites at the open

99 sides of the linkers. The adsorption sites above the benzene rings of the linkers are not as significantly

100 occupied as in pristine MOF-FA, not even at the highest pressures.
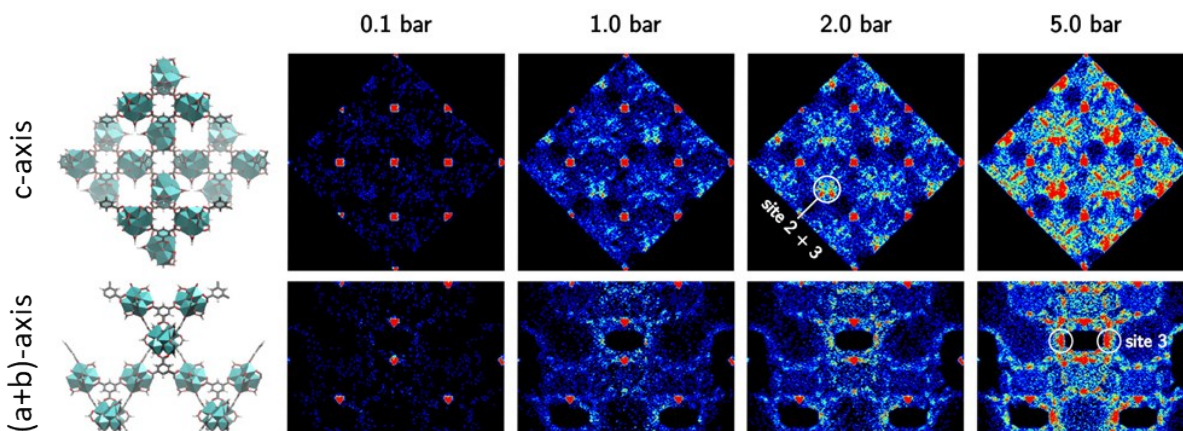
101

102 Figure S11: Density of the adsorbed CO_2 molecules in MOF-FA-def3 at 300 K projected on a plane orthogonal to the c-axis and
103 the (a + b)-axis of the conventional unit cell. The CO_2 molecules are represented by the positions of the carbon atoms.

104 Table S6: Simulated adsorption enthalpies for MOF-FA, MOF-TFA and MOF-FA with 1 and 3 defect(s), respectively.

| Pressure (bar)	MOF-FA	MOF-FA-def1	MOF-FA-def3	MOF-TFA
0.010	-45.2	-43.7	-41.2	-44.8
0.025	-41.6	-41.2	-39.2	-40.6
0.050	-35.2	-36.2	-35.3	-34.3
0.075	-30.1	-31.8	-31.7	-30.3
0.10	-26.8	-28.5	-28.8	-27.9
0.25	-20.5	-21.0	-21.5	-23.9
0.50	-19.1	-19.0	-19.4	-23.1
0.75	-18.7	-18.6	-18.9	-22.9
1.00	-18.6	-18.4	-18.7	-22.8
1.25	-18.4	-18.3	-18.6	-22.7
1.50	-18.4	-18.2	-18.5	-22.6
1.75	-18.3	-18.2	-18.4	-22.5
2.00	-18.2	-18.1	-18.4	-22.4
2.50	-18.1	-18.0	-18.3	-22.1
5.00	-17.4	-17.5	-17.9	-20.7
7.50	-16.9	-17.0	-17.5	-19.4
10.0	-16.5	-16.6	-17.1	-18.6

105
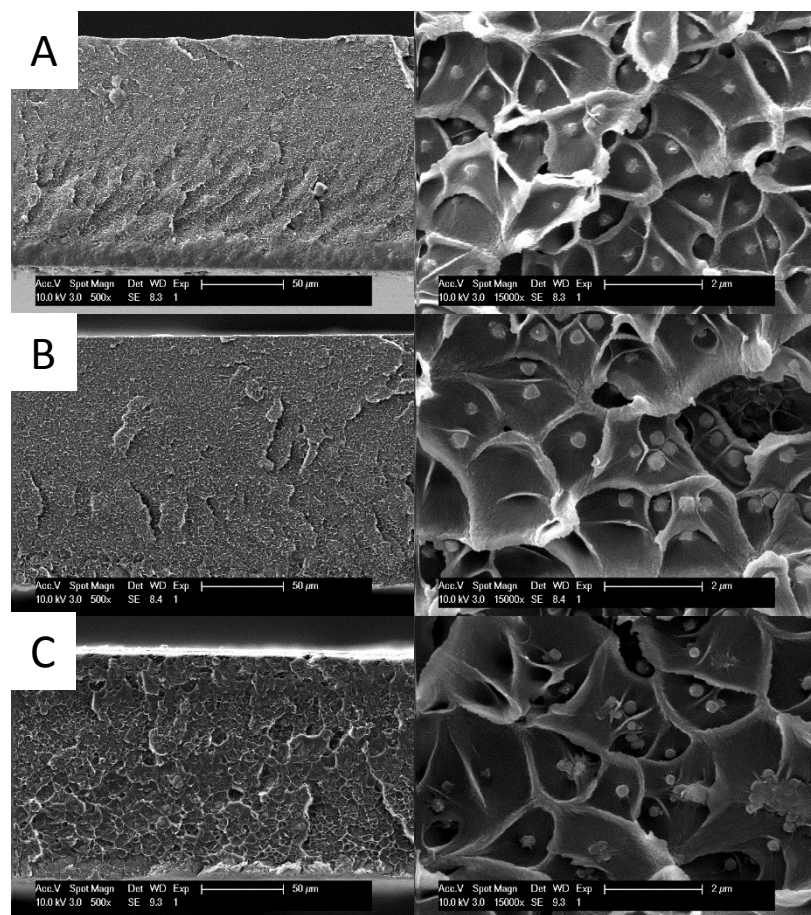
Figure S12: SEM cross-sections of A) MMM-FA, B) MMM-BA and C) MMM-TFA. All MMMs contain 10 wt.% MOF.

109
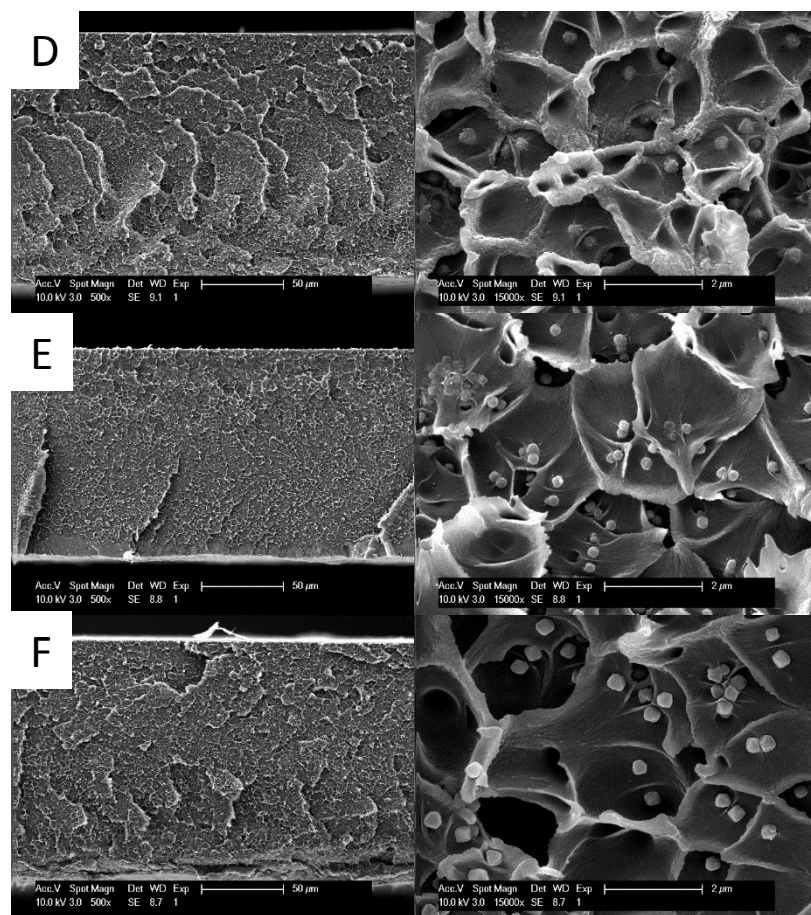
Figure S13: SEM cross-sections of D) MMM-GA, E) MMM-His and F) MMM-Li$_2$SO$_4$. All MMMs contain 10 wt.% MOF.

111

112   Table S7: Thermal analysis of all membranes.

	Glass transition temperature (T$_g$, °C)	Decomposition temperature (T$_d$, °C)	Weight % MOF according to TGA
Matrimid	312	555	-
MMM-FA	324	548	10
MMM-GA	320	547	9
MMM-BA	322	550	8
MMM-His	322	553	8
MMM-TFA	320	552	8
MMM-Li$_2$SO$_4$	322	-	-

113

114

115

116

117

118
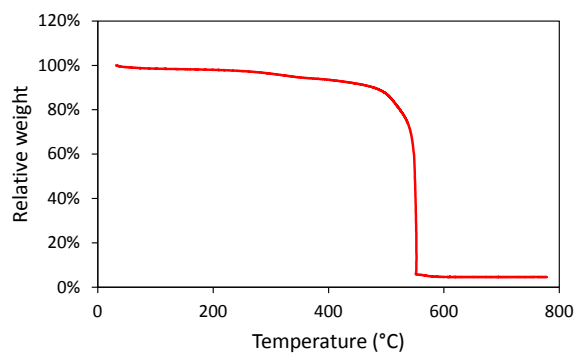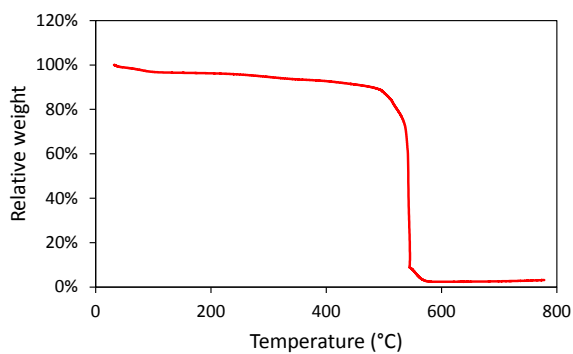
119
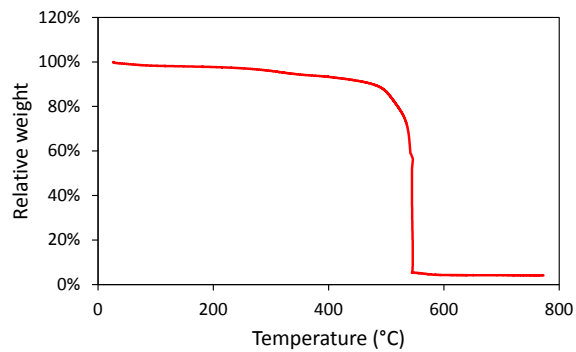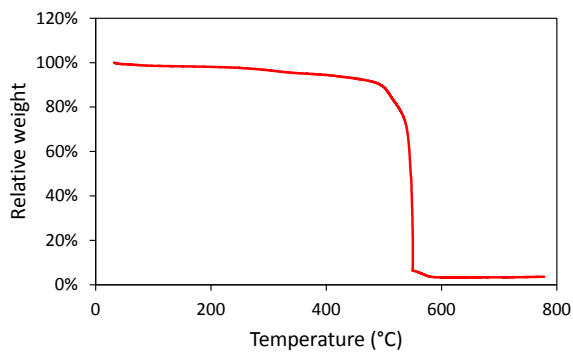
120
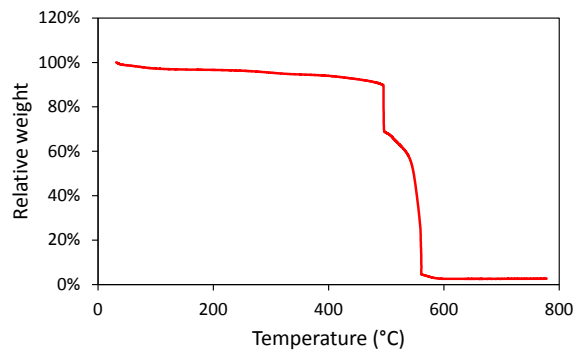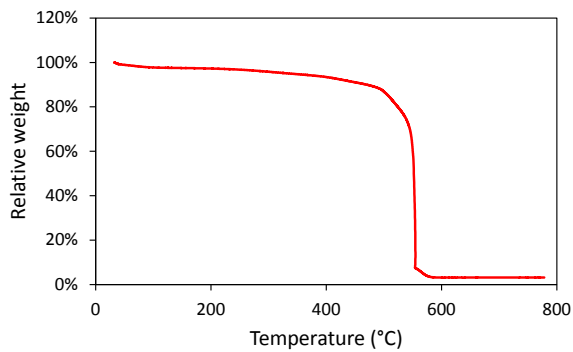
121

122 Figure S14: TGA traces of MMM-FA (top left), MMM-TFA (top right), MMM-BA (middle left), MMM-GA (middle right), MMM-His
123 (bottom left) and MMM-Li$_2$SO$_4$ (bottom right).

124 Exo Down   Universal V4.3A
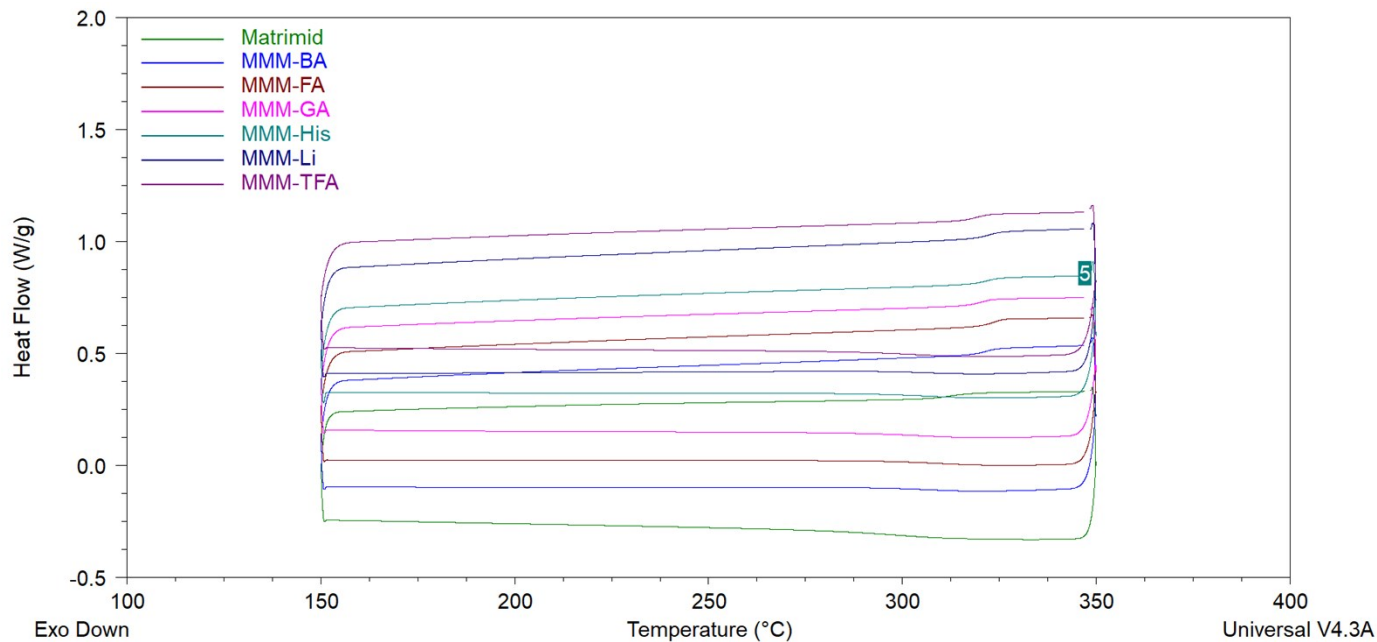
125 Figure S15: DSC traces of all MMMs and Matrimid.
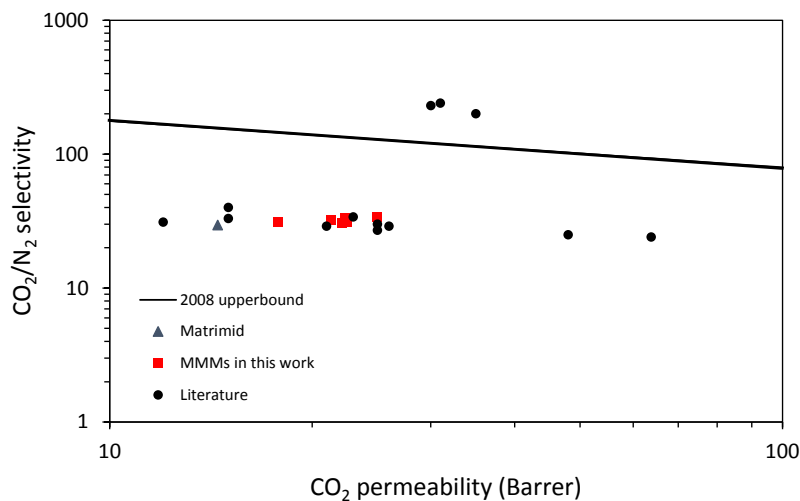
126

127 Figure S16: Comparison of the performance of the MMMs produced in this work with literature[76,89–92] and the 2008 Robeson
128 CO_2/N_2 upper bound.

129

130

131

132

133

134

135

136 Table S8: Correlation factors between MOF parameters.

	Correlation of MOF parameters	273 K		293 K		313 K		BET surface area	Pore volume	$Q_{st,0}$	$Q_{st,15}$	$Q_{st,30}$
		CO_2 uptake (50 mbar)	CO_2 uptake (1000 mbar)	CO_2 uptake (50 mbar)	CO_2 uptake (1000 mbar)	CO_2 uptake (50 mbar)	CO_2 uptake (1000 mbar)					
273 K	CO_2 uptake (50 mbar)	1.00	0.22	0.85	0.81	0.95	0.78	0.54	0.50	0.77	0.86	0.67
	CO_2 uptake (1000 mbar)		1.00	-0.25	0.63	-0.09	0.70	0.82	0.83	0.03	0.53	0.66
293 K	CO_2 uptake (50 mbar)			1.00	0.51	0.96	0.44	0.17	0.10	0.61	0.54	0.21
	CO_2 uptake (1000 mbar)				1.00	0.64	0.98	0.64	0.61	0.36	0.92	0.83
313 K	CO_2 uptake (50 mbar)					1.00	0.59	0.29	0.24	0.73	0.69	0.43
	CO_2 uptake (1000 mbar)						1.00	0.69	0.66	0.36	0.85	0.81
	BET surface area							1.00	0.99	0.45	0.67	0.61
	Pore volume								1.00	0.48	0.67	0.67
	$Q_{st,0}$									1.00	0.59	0.53
	$Q_{st,15}$										1.00	0.90
	$Q_{st,30}$											1.00

137

138 Table S9: Correlation factors between membrane parameters.

Correlation of membrane parameters	$\alpha_{15/85}$	$\alpha_{50/50}$	α_{ideal}	$P_{15/85}$	$P_{50/50}$	$P_{100/0}$	CO_2 uptake (1 bar)	CO_2 uptake (2 bar)	CO_2 uptake (3 bar)	CO_2 uptake (4 bar)	CO_2 uptake (5 bar)
$\alpha_{15/85}$	1.00	0.89	-0.97	0.58	0.74	0.55	0.42	0.36	0.38	0.41	0.39
$\alpha_{50/50}$		1.00	-0.80	0.73	0.75	0.74	0.03	-0.05	-0.04	-0.01	-0.03
α_{ideal}			1.00	-0.39	-0.59	-0.37	-0.56	-0.49	-0.49	-0.52	-0.47
$P_{15/85}$				1.00	0.95	0.98	-0.18	-0.21	-0.20	-0.20	-0.16
$P_{50/50}$					1.00	0.90	0.14	0.11	0.11	0.10	0.13
$P_{100/0}$						1.00	-0.27	-0.33	-0.33	-0.34	-0.31
CO_2 uptake (1 bar)							1.00	0.98	0.95	0.92	0.87
CO_2 uptake (2 bar)								1.00	0.99	0.97	0.94
CO_2 uptake (3 bar)									1.00	1.00	0.98
CO_2 uptake (4 bar)										1.00	0.99
CO_2 uptake (5 bar)											1.00

139

140